Inorganic Chemistry

Article

Cite This: Inorg. Chem. 2019, 58, 13815−13825

pubs.acs.org/IC

Magnetic Properties of a Family of [$Mn^{III}_4Ln^{III}_4$] Wheel Complexes: An Experimental and Theoretical Study

Gavin A. Craig,[†,∥] Gunasekaran Velmurugan,[‡] Claire Wilson,[†] Rafael Valiente,[§] Gopalan Rajaraman,*[,‡] and Mark Murrie*[,†]

[†]WestCHEM, School of Chemistry, University of Glasgow, Glasgow G12 8QQ, United Kingdom

[‡]Department of Chemistry, Indian Institute of Technology Bombay, Powai, Mumbai, Maharashtra 400 076, India

[§]Física Aplicada, Facultad de Ciencias, Universidad de Cantabria-IDIVAL, Avda. Los Castros s/n, 39005 Santander, Spain

Supporting Information

ABSTRACT: The chelating ligand 1,3-bis(tris-(hydroxymethyl)methylamino)propane (H_6L) has been used to synthesize a family of octanuclear heterometallic complexes with the formula $(NMe_4)_3[Mn_4Ln_4(H_2L)_3(H_3L)(NO_3)_{12}]$ (Ln = La (**1**), Ce (**2**), Pr (**3**), Nd (**4**)). Encapsulation by the ligand causes the Mn(III) centers to lie in an unusually distorted ($\sim C_{2v}$) environment, which is shown by density functional theory and complete active space self-consistent field calculations to impact on the magnetic anisotropy of the Mn(III) ion. The theoretical study also supports the experimental observation of a ferromagnetic superexchange interaction between the Mn(III) ions in **1**, despite the ions being separated by the diamagnetic La(III) ion. The optical properties of the compounds show that the distortion of the Mn(III) ions leads to three broad absorption bands originating from the transition metal ion, while the Nd(III) containing complex also displays some weak sharp features arising from the lanthanide f−f transitions.

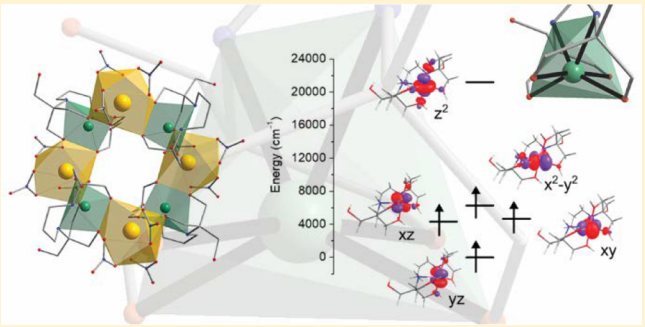

INTRODUCTION

The molecular approach to the synthesis of nanomagnets offers a wide range of possibilities to tailor the functionality of the final compound, from the design of single-ion magnets,[1−3] to the building-block construction of single chain magnets,[4−6] and the directed assembly of molecular qubits.[7−10] Although the majority of initial research in the field of molecular nanomagnets studied compounds that contained only 3d transition metal (TM) ions,[11] the past decade has seen a lot of effort invested in trying to incorporate TM ions and lanthanide ions into metal complexes.[12,13] Lanthanide ions are attractive for this purpose because their spin−orbit coupling is a first order effect, which can lead to high magnetic anisotropy.[14,15]

3d-4f compounds have also been used as magnetic coolers,[16−18] and techniques such as inelastic neutron scattering (INS) and high field electron paramagnetic resonance (HF-EPR) spectroscopy have helped to elucidate the nature of magnetic exchange interactions between the 3d and 4f centers.[19−21] Advantageously for systematic studies, the well-known lanthanide contraction often allows a particular lanthanide site to be occupied by several other members of the rare earth series, such that it is possible to synthesize families of isostructural complexes.[22−28] The decrease in the ionic radii of the Ln(III) ion as the series is crossed has also allowed the targeted substitution of TM ions for Ln(III) ions of higher magnetic anisotropy.[29,30]

The use of amino-polyalcohol ligands is a particularly successful approach to synthesize such 3d-4f complexes, thanks to the flexibility of the ligand backbone.[31] In previous work, we have shown how the ligand 1,3-bis(tris(hydroxymethyl)-methylamino)propane (H_6L, Scheme 1) can be used to build up polynuclear assemblies of 3d TM ions.[32−35] Using H_6L, both serendipitous assembly and directed synthesis were employed to synthesize novel compounds, with the most spectacular example being a $[Mn_{18}Cu_6]$ complex built in a stepwise fashion, starting from a monomeric precursor complex of Cu(II) with H_6L.[33] Regardless of the approach, H_6L has a tendency to encapsulate one 3d TM ion in the coordination pocket defined by the propane-1,3-diyldiimino backbone, leaving the flexible hydroxymethyl arms to link to other metal ions and increase the nuclearity of the final

Scheme 1. Ligand 1,3-Bis(tris(hydroxymethyl)methylamino)propane (H_6L)

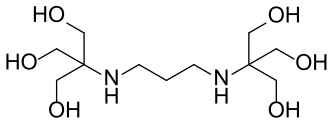

Received: May 31, 2019
Published: October 7, 2019

DOI: 10.1021/acs.inorgchem.9b01592
Inorg. Chem. 2019, 58, 13815−13825

Table 1. Selected Crystallographic Data for Compounds 1−4

	1	2	3	4
formula	$C_{60}H_{143}Mn_4N_{23}La_4O_{65}$	$C_{60}H_{143}Mn_4N_{23}Ce_4O_{65}$	$C_{60}H_{143}Mn_4N_{23}Pr_4O_{65}$	$C_{60}H_{143}Mn_4N_{23}Nd_4O_{65}$
crystal system	tetragonal	tetragonal	tetragonal	tetragonal
space group	$P\text{-}42_1/c$	$P\text{-}42_1/c$	$P\text{-}42_1/c$	$P\text{-}42_1/c$
a/Å	18.834(1)	18.812(1)	18.767(2)	18.761(1)
b/Å	18.834(1)	18.812(1)	18.767(2)	18.761(1)
c/Å	15.522(1)	15.508(1)	15.461(2)	15.469(1)
V/Å^3	5506.2(2)	5488.1(7)	5445.4(11)	5444.5(6)
Z	2	2	2	2
D(calc)/g cm^{-3}	1.81	1.82	1.84	1.84
μ/mm^{-1}	2.07	2.18	2.32	2.43
F(000)	3024	3032	3040	3048
crystal size/mm	0.18 × 0.04 × 0.04	0.02 × 0.03 × 0.09	0.30 × 0.40 × 0.40	0.04 × 0.08 × 0.09
temperature/K	100	100	100	100
radiation/Å	0.71073	0.71073	0.71073	0.71073
total reflections	22 009	43 855	70 695	75 906
unique data	6305	6314	6259	6247
R(int)	0.019	0.095	0.074	0.032
Nref, Npar	6284, 438	5635, 381	5893, 377	6163, 391
R_1	0.019	0.035	0.026	0.013
wR_2	0.016	0.066	0.064	0.034
S	0.98	1.05	1.10	1.07
Flack parameter	−0.033(4)	−0.003(10)	−0.003(6)	0.001(2)

complex.[36] A recent example showed how this ligand can be used to synthesize $[Ln_2Cu_3]$ complexes (Ln = Gd, Tb, Dy, Ho, or Er) displaying slow relaxation of the magnetization, which could be tuned by varying the auxiliary anionic ligands present.[37] In this Article, we report the synthesis and characterization of a family of octanuclear, wheel-shaped 3d-4f complexes $(NMe_4)_3[Mn_4Ln_4(H_2L)_3(H_3L)(NO_3)_{12}]$, for the early members of the lanthanide series [Ln = La (**1**), Ce (**2**), Pr (**3**), Nd (**4**)]. A superexchange interaction is found between the Mn(III) ions in compound **1**, despite taking place through a diamagnetic La(III) ion. A mechanism for this interaction is proposed on the basis of density functional theory (DFT) and complete active space self-consistent field (CASSCF) calculations.

EXPERIMENTAL SECTION

Synthesis. Reagents were used as purchased from Sigma-Aldrich, with no further purification. All manipulations were performed under aerobic conditions.

General Procedure To Synthesize Compounds 1−4. 1,3-Bis(tris(hydroxymethyl)methylamino)propane (0.300 g, 1.06 mmol) and tetramethylammonium hydroxide pentahydrate (0.193 g, 1.06 mmol) were mixed and stirred in MeOH (30 mL) at ∼60 °C. After 20 min, $Mn(NO_3)_2{\cdot}4H_2O$ (0.522 g, 2.07 mmol) was added, and the resulting burgundy solution left to stir. After 1 h, $Ln(NO_3)_3{\cdot}6H_2O$ (1.06 mmol) was added, giving a dark purple solution. After 4 h the solution was cooled to room temperature, before being filtered and left to slowly evaporate. Purple crystals suitable for X-ray diffraction formed after 4 days and were filtered and dried in air.

*$(NMe_4)_3[Mn_4La_4(H_2L)_3(H_3L)(NO_3)_{12}]{\cdot}(H_2O){\cdot}4(MeOH)$ (**1**·(H_2O)·4(MeOH))*. Yield (based on La(III) salt): 0.195 g, 24.5%. IR (neat, υ = cm^{-1}) = 1479 (m), 1435 (s), 1316 (s), 1282 (m), 1092 (s), 1024 (s), 1001 (s), 677 (m). Elemental analysis calcd (%) for $C_{56}H_{141}La_4Mn_4N_{23}O_{68}$ (**1**·8H_2O): C 22.42, H 4.74, N 10.74; found: C 22.10, H 4.46, N 10.53. Mn:La ratio from SEM-EDX: 50.6(14):49.4(14). The presence of the water molecules is accounted for by TGA (see SI Figure S1).

*$(NMe_4)_3[Mn_4Ce_4(H_2L)_3(H_3L)(NO_3)_{12}]{\cdot}(H_2O){\cdot}4(MeOH)$ (**2**·(H_2O)·4(MeOH))*. Yield (based on Ce(III) salt): 0.232 g, 28.9%. IR (neat, υ = cm^{-1}) = 1488 (m), 1480 (m), 1437 (s), 1303 (s), 1284 (m), 1024 (s), 1001 (s), 678 (s). Elemental analysis calcd (%) for $C_{56}H_{143}Ce_4Mn_4N_{23}O_{69}$ (**2**·9H_2O): C 22.25, H 4.77, N 10.66; found: C 22.10, H 4.52, N 10.33. Mn:Ce ratio from SEM-EDX: 49.8(5):50.2(5). The presence of the water molecules is accounted for by TGA (see SI Figure S2).

*$(NMe_4)_3[Mn_4Pr_4(H_2L)_3(H_3L)(NO_3)_{12}]{\cdot}(H_2O){\cdot}4(MeOH)$ (**3**·(H_2O)·4(MeOH))*. Yield (based on Pr(III) salt): 0.219 g, 27.6%. IR (neat, υ = cm^{-1}) = 1479 (m), 1425 (m), 1302 (s), 1091 (w), 1016 (s), 1002 (s), 677 (s). Elemental analysis calcd (%) for $C_{56}H_{141}Mn_4N_{23}O_{68}Pr_4$ (**3**·8H_2O): C 22.38, H 4.73, N 10.72; found: C 22.95, H 4.66, N 10.31. Mn:Pr ratio from SEM-EDX: 48.4(10):51.6(10). The presence of the H_2O molecules is accounted for by TGA (see SI Figure S3).

*$(NMe_4)_3[Mn_4Nd_4(H_2L)_3(H_3L)(NO_3)_{12}]{\cdot}(H_2O){\cdot}4(MeOH)$ (**4**·(H_2O)·4(MeOH))*. Yield (based on Nd(III) salt): 0.200 g, 24.8%. IR (neat, υ = cm^{-1}) = 1435 (m), 1430 (m), 1302 (s), 1091 (w), 1017 (s), 1001 (s), 677 (s). Elemental analysis calcd (%) for $C_{56}H_{143}Mn_4N_{23}Nd_4O_{69}$ (**4**·9H_2O): C 22.13, H 4.74, N 10.60; found: C 22.27, H 4.57, N 10.42. Mn:Nd ratio from SEM-EDX: 49.7(5):50.3(5). The presence of the H_2O molecules is accounted for by TGA (see SI Figure S4).

Physical Measurements. *Thermogravimetric Analysis (TGA).* Measurements for **1**−**4** were carried out using a TA Instruments Q600 thermogravimetric analyzer over the temperature range of 20−400 °C with a heating rate of 5 °C min^{-1} under an Ar atmosphere.

Single Crystal X-ray Diffraction. Crystallographic data were collected for compounds **1**−**4** at 100 K using Mo Kα radiation (λ = 0.71073 Å) on a Rigaku AFC12 goniometer equipped with a (HG) Saturn724+ detector mounted on an FR-E+ SuperBright rotating anode generator with HF Varimax optics (100 μm focus).[38] The structure of **1** was solved using SUPERFLIP[39] and refined against F^2 using CRYSTALS.[40] The structures of **2**−**4** were solved within Olex2[41] using the SHELXT structure solution program and refined with ShelXL using least-squares minimization (Table 1).[42,43] In all cases, the hydrogen atoms of the disordered MeOH molecule, the H_2O molecule at the center of the wheel, and a disordered charge-balancing proton that is most likely to be on an O-atom of the ligand (see discussion below) were not included in the model. All non-hydrogen atoms were refined anisotropically. The cif files for these structures have been submitted to the Cambridge Structural Database: CCDC 1874195−1874198. These data can be obtained free of charge from the Cambridge Crystallographic Data Centre via www.ccdc.cam.ac.uk/data_request/cif.

DOI: 10.1021/acs.inorgchem.9b01592
Inorg. Chem. 2019, 58, 13815−13825

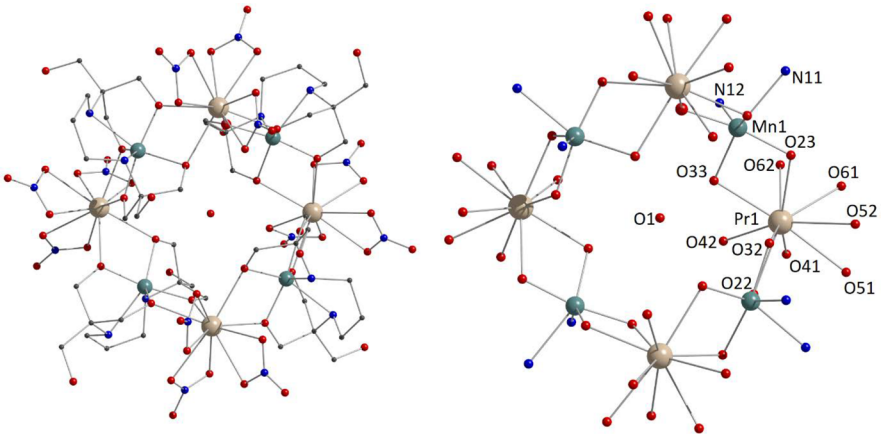

Figure 1. (left) View of the $[Mn_4Pr_4]^{3-}$ ring in compound **3**, with the water molecule at the center of the ring shown. (right) View of the ring showing atoms bound to metal ions only and the water molecule, with crystallographically independent atoms labeled. Hydrogen atoms are omitted for clarity.

Scanning Electron Microscopy with Energy Dispersive X-ray Spectroscopy (SEM-EDX). Crystals of compounds **1**−**4** were deposited on conductive carbon tabs mounted on an aluminum stub. The samples were coated with Pd using a Polaron SC7640 sputter coater. The SEM-EDX experiments were then performed with a Philips XL30 ESEM tungsten filament electron microscope. Representative images are given in SI Figures S5−S8.

Powder X-ray Diffraction. The powder X-ray patterns for compounds **1**−**4** (see SI Figures S9−S12) were collected on a PANalytical XPert MPD, with Cu Kα1 radiation at ambient temperature over a range of $5° < 2\theta < 50°$ using a step size of 0.0167°. Calculated patterns for **1**−**4** were generated from Mercury[44] using the cif of the corresponding crystal structure at 100 K.

Magnetic Studies. Direct current (dc) magnetic measurements were performed on polycrystalline samples of **1**−**3** constrained in eicosane on an MPMS-XL SQUID. The direct current (dc) measurements were carried out in the temperature range 290−1.8 K under an applied field of 1000 Oe. Data were corrected for the diamagnetism of the compound and for the diamagnetic contributions of the sample holder and eicosane through measurements. Alternating current (ac) measurements were performed on the same samples, with a drive field of 3 Oe at 1.8 K, over the frequency range 1−1267 Hz, under various applied dc fields as given in the text. The dc measurements performed on **4** were carried out on an MPMS-XL SQUID at the Servicio General de Apoyo a la Investigación-SAI, Universidad de Zaragoza, under a field of 1000 Oe in the temperature range 300 to 1.9 K. The field dependence of χ'' was measured at 2 K over the range H_{dc} = 0−5000 Oe at a frequency of 125 Hz.

Computational Details. All calculations were carried out with the Gaussian09 program package[45] using the UB3LYP functional[46] with the TZV basis set.[47,48] Here we have used Noodleman's broken symmetry (BS) approach, derived from a spin-unrestricted reference wave function to estimate the energy of all spin-states, except that of the high-spin state.[49] This approach, along with the widely used exchange-correlation functional, B3LYP, provides a good numerical estimate of exchange coupling constants compared to experiment.[50−57] There are many approaches to compute exchange interactions from the broken symmetry energies, and here we adopted the pairwise interaction model to compute the exchange coupling. The chosen computational setup, together with this model, yields a good estimate of the coupling constants in many dinuclear and polynuclear complexes. For the calculation of 1,3-exchange mediated via Ln(III) ions, earlier studies show that this method yields a good numerical estimate of J values.[58−60] Both the functional and the basis sets are chosen based on our earlier method of assessment for [3d-Gd-3d] and [Gd-radical] pairs.[60,61] The following Hamiltonian is used to estimate the exchange interaction (J).

$$J = \frac{(E_{BS} - E_{HS})}{2S_1S_2 + S_2}$$

All the first principle calculations have been performed in the ORCA 3.0.3 program package.[62] We employed the def2-TZVP basis set for Mn, N, O, and def2-SVP for the rest of the atoms. In order to speed up the integral calculations, we have used the RI (resolution of identity) approximation along with the given auxiliary basis sets. We employed these orbitals to start the state averaged complete active space self-consistent field (SA-CASSCF) calculations.[58−60] The active space in this calculation is composed of four d-electrons of Mn in five d-orbitals, i.e., CAS(4,5). Using this active space, we have computed 5 quintet and 35 triplet roots in the CI (configuration interaction) procedure. To incorporate the dynamic correlation, we employed N-electron valence perturbation theory (NEVPT2)[63−65] on top of the CASSCF wave function. The def2-TZVP/C for Mn, N, O and def2-SVP/C auxiliary basis set for the other atoms have been used with the Trafostep RIMO approximation. Here, the Trafostep RIMO approximation was used for integral transformation in the CASSCF calculations while the Fock operators are still calculated in the standard way using four index integrals. To account for the scalar relativistic effects, the zeroth-order regular approximation (ZORA) method was used both in the Hamiltonian as well as in the basis functions during all calculations. The zero-field splitting parameters (D and E) were calculated both from second-order perturbation theory and an effective Hamiltonian approach (EHA).[66] The spin−orbit coupling effects were incorporated by using the quasi-degenerate perturbation theory (QDPT) approach.[67] As our systems and model size are very large, we have restricted our calculations to a CAS (4,5) reference space and have not included the double-shell effect, the effects of which are known to be particularly minimal if NEVPT2 is employed.[68,69]

Optical Properties. Room temperature electronic absorption spectra for **1**−**4** were collected using a Varian Cary 6000i UV−vis-NIR double-beam spectrophotometer equipped with an integrating sphere (DRA 1800).

RESULTS AND DISCUSSION

Synthesis. Compounds **1**−**4** were synthesized with the same general procedure, and their identity established through single crystal X-ray crystallography, IR spectroscopy, powder X-ray diffraction, thermogravimetric analysis, and elemental analysis. The compounds described here contain the four earliest members of the lanthanide series, spanning La(III) to Nd(III). We were not able to isolate analogous wheels containing later, more magnetically anisotropic lanthanide ions such as Tb(III) or Dy(III). X-ray structure analyses of **1**−**4**

DOI: 10.1021/acs.inorgchem.9b01592
Inorg. Chem. 2019, 58, 13815−13825

(vide infra) show that the Ln(III) ions are ten-coordinate. It is possible that the lanthanide contraction prevents the formation of the wheels for the smaller Ln(III) ions in this coordination environment. A similar phenomenon was observed in a family of bell-shaped $Mn_{11}Ln_2$ complexes that could only be synthesized with the early members of the lanthanide series.[70]

Description of the Crystal Structures. The complexes reported here are isostructural, and crystallize in the tetragonal space group $P-42_1/c$ (Table 1). The asymmetric unit consists of one-quarter of the $[Mn_4Ln_4(H_2L)_3(H_3L)(NO_3)_{12}]^{3-}$ wheel, one-quarter of a disordered water molecule lying on a −4 site around which the wheel is assembled, one MeOH molecule disordered over two sites, and part of two crystallographically independent NMe_4^+ cations which lie on a −4 and a 2-fold axis of which 1/4 and 1/2 are unique, respectively. For the sake of brevity, hereafter only the structure of **3** (Ln = Pr) will be described in detail.

The $[Mn_4Pr_4]^{3-}$ ring contains an arrangement of alternating Mn(III) and Pr(III) ions (Figure 1). The oxidation state of the transition metal was determined by bond valence sum calculations in PLATON[71] and consideration of charge balance. The Mn(III) ions are hexacoordinate and are encapsulated by the partially deprotonated bis-tris propane ligand (Figure 2). The coordination sphere of the Mn(III) ion

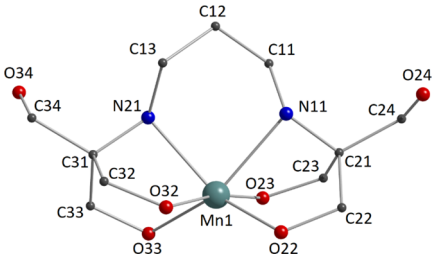

Figure 2. View of the encapsulation of the Mn(III) ion by the bis-tris propane ligand. Hydrogen atoms are omitted for clarity.

is heavily distorted away from ideal octahedral symmetry and far from the usual uniaxial Jahn−Teller distortion of this ion. There are two very long Mn−N bonds (Mn1−N11 and Mn1−N12 are 2.319(4) and 2.242(4) Å, respectively), and the angle between them deviates from the ideal 90° (83.2(1)°). The Mn−O bond lengths range from 1.892(3) to 2.076(3) and average 1.950(3) Å. The largest deviation for the *cis*-angles is found for the O22−Mn1−O33 angle, which measures 131.64(12)°. This distortion around the Mn(III) ion is important for the magnetic and optical properties observed for these compounds (vide infra).

The Mn(III) ions are linked on either side to the adjacent Pr(III) ions through the $\eta^2{:}\eta^2{:}\mu$ arms of the ligand. There are two different Mn(III)···Pr(III) distances alternating around the ring, of 3.523(1) and 3.565(1) Å. The Pr(III) ions are deca-coordinate, with a coordination sphere consisting only of oxygen atoms, and are best described as displaying C_{2v} symmetry (see the SI, Table S1). The bridging arms of the chelating ligands provide four of the oxygen atoms, and the remaining six sites are occupied by two oxygen donors each from three NO_3^- ligands. The average Ln−O bond length decreases with increasing number of 4f electrons, consistent with the lanthanide contraction (SI Table S3).[72] There is a significant curvature of the ring (Figure 3), such that it resembles a $[Fe_4Dy_4]$ ring assembled with triethanolamine,[21] which also formed around a central H_2O molecule, and a

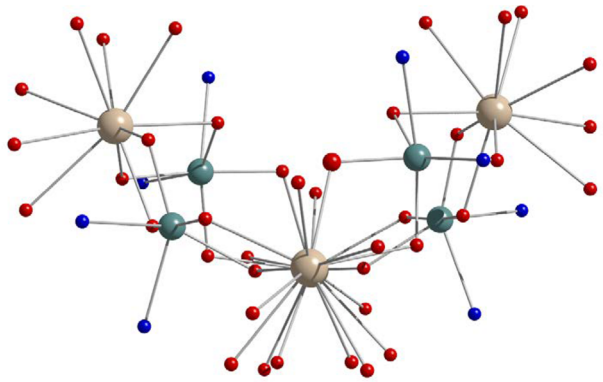

Figure 3. Side view of the $[Mn_4Pr_4]$ ring in **3**, showing only atoms bound to metal ions. Color scheme as in Figure 1.

family of $[Mn_4Ln_4]$ wheels that contained heavier lanthanide ions linked with *N*-*n*-butyl-diethanolamine.[26,73] There is a hydrogen bonding interaction between O33 and the H_2O molecule around which the wheel is assembled, measuring 2.812(3) Å (O33···O1).

For charge balance, three of the four H_6L proligands must be quadruply deprotonated (H_2L^{4-}), while the other ligand is triply deprotonated (H_3L^{3-}), hence leading to the the formulation of the anionic wheel as $[Mn_4Ln_4(H_2L)_3(H_3L)(NO_3)_{12}]^{3-}$. In all four ligands, both N atoms remain protonated, as are the O atoms O24 and O34, which belong to terminal alcohol arms found at the edge of the ring. In three of the ligands, all four of the bridging alkoxo- arms must be deprotonated, to give the H_2L^{4-} form of the ligand. In the fourth ligand, a proton must be shared over these alkoxo- arms to give the H_3L^{3-} form. Considering the geometries around the remaining alkoxo- O atoms, it is likely that O23 and O32 are both deprotonated, as the O23 and O32 atoms lie in the planes defined by Mn1−C23−Pr1 and Mn1−C32−Pr1, respectively (see the SI). In contrast, O22 and O33 are both found out of the planes defined by Mn1−C22−Pr1 and Mn1−C33−Pr1, at distances of 0.396 and 0.488 Å, respectively (see SI Figures S13−S16). The charge balancing proton is most likely to be found disordered over these two atoms and their four symmetry equivalent counterparts in the ring.

Magnetic Properties. The magnetic properties of compounds **1**−**4** were measured on polycrystalline samples, with their phase purity demonstrated by powder X-ray diffraction (see SI Figures S9−S12). Figure 4 shows the temperature dependence of $\chi_M T$ for **1**−**4**. The values of $\chi_M T$ at 280 K are 11.8, 15.1, 18.6, and 18.3 $cm^3\ mol^{-1}\ K$ (for **1**−**4**, respectively), consistent with four uncoupled Mn(III) ions (S = 2, g = 2, $\chi_M T_{calc}$ = 12.0 $cm^3\ mol^{-1}\ K$) and four uncoupled Ln(III) ions. On lowering the temperature to 50 K, **2**−**4** predominantly show a decrease in $\chi_M T$, which is most likely caused by the depopulation of the m_J states. This depopulation can effectively mask any coupling between the Mn(III) ions and the Ln(III) ions. The decrease in $\chi_M T$ for **3** is continual, reaching a minimum of 10.3 $cm^3\ mol^{-1}\ K$ at 1.8 K. Compounds **2** and **4** enter a plateau below 30 K, before increasing to reach respective maxima at 8 and 6 K of 14.1 and 17.0 $cm^3\ mol^{-1}\ K$. Beyond this point, $\chi_M T$ decreases for both compounds, reaching 9.3 $cm^3\ mol^{-1}\ K$ at 1.8 K (**2**) and 16.4 $cm^3\ mol^{-1}\ K$ at 1.9 K (**4**). The observed small increases in $\chi_M T$ at low temperature could be due to ferromagnetic interactions between the spin centers in the ring, with the final decrease in

DOI: 10.1021/acs.inorgchem.9b01592
Inorg. Chem. 2019, 58, 13815−13825

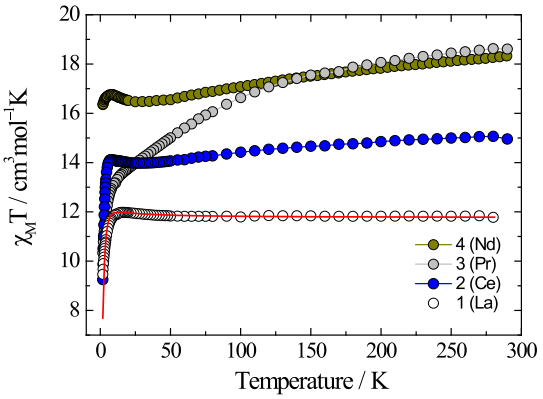

Figure 4. Temperature dependence of $\chi_M T$ for compounds **1** (La) to **4** (Nd), measured under a dc field of 1000 Oe. The solid red line corresponds to a simulation of the data (see the text for details), and the other lines are guides for the eye.

$\chi_M T$ caused by antiferromagnetic intermolecular interactions and/or zero-field splitting (ZFS) of the Mn(III) ion. Compound **1** contains the diamagnetic La(III) ion, and so the $\chi_M T$ curve reveals the magnetic properties that arise from the presence of the Mn(III) ions only. On lowering the temperature, $\chi_M T$ for **1** remains constant until 50 K, where it begins to increase, reaching a maximum at 14 K of 12.0 cm^3 mol^{-1} K, before decreasing at lower temperatures to a minimum of 9.5 cm^3 mol^{-1} K at 1.8 K. The data for **1** were modeled with the program PHI,[74] according to the Hamiltonian:

$$\hat{H} = -2J(\hat{S}_a\hat{S}_b + \hat{S}_b\hat{S}_c + \hat{S}_c\hat{S}_d + \hat{S}_d\hat{S}_a) + g\mu_B\vec{B}\sum_{i=1}^{4}\hat{S}_i$$

where the subscripts distinguish between the Mn(III) ions. In order to obtain a good match to the data at low temperature, an intermolecular interaction, zJ, was included using the mean field approximation: there are eight strong intermolecular hydrogen bonding interactions between the rings through O34−H15···O24′ (four donor interactions and four acceptor interactions for each ring; for compound **1**, this O···O distance is 2.787(2) Å, see the SI). The simulation shown in Figure 4 has J = +0.22 cm^{-1} and zJ = −0.045 cm^{-1}. The exchange between two transition metal ions as mediated by the closed-shell Ln(III) ions [La(III) at one end of the series, or Lu(III) at the other] has been found to be weak.[75−77] DFT calculations were previously used to show the exchange between Mn(III) ions across Y(III) in a Mn_8Y_8 disc to be J = +0.43 cm^{-1},[78] while antiferromagnetic coupling was observed in a linear Ni−La−Ni compound (J = −0.978 cm^{-1}),[79] and antiferromagnetic coupling of J = −0.45 cm^{-1} was determined between Fe(III) ions through Gd(III) ions in a $Fe_{10}Gd_{10}$ disc.[80] An alternative to intermolecular antiferromagnetic interactions as an explanation for the decrease in $\chi_M T$ at low temperatures could be the ZFS associated with the Mn(III) ions. However, any attempt to include a contribution for the ZFS of the Mn(III) ion in the simulations was unsuccessful, because it overcompensated the weak intramolecular coupling interaction and negated the increase in $\chi_M T$ that is observed on lowering the temperature. To confirm the suitability of the simulated intra- and intermolecular exchange interactions found for compound **1**, and to investigate the possible ZFS associated with the Mn(III) ions, we used DFT and CASSCF calculations (vide infra).

The magnetization of compounds **1**−**4** was measured as a function of an applied field over the range 0−5 T at 2 and 5 K (Figures S19−S22). All of the compounds show an increase in $M/N\beta$ with the magnetic field, although none reaches saturation, presumably due to the lack of a well-defined ground state causing the population of low-lying excited states (vide infra) and the presence of magnetic anisotropy. The alternating current (ac) magnetic measurements performed on **1**−**4** for H_{dc} = 0 Oe (Figures S23−S26) showed no appreciable out-of-phase component to the susceptibility (χ''). The lack of a signal in χ'' can be caused by efficient quantum tunneling of the magnetization (QTM), which may be disrupted by the application of an external dc field. Recent papers have reported

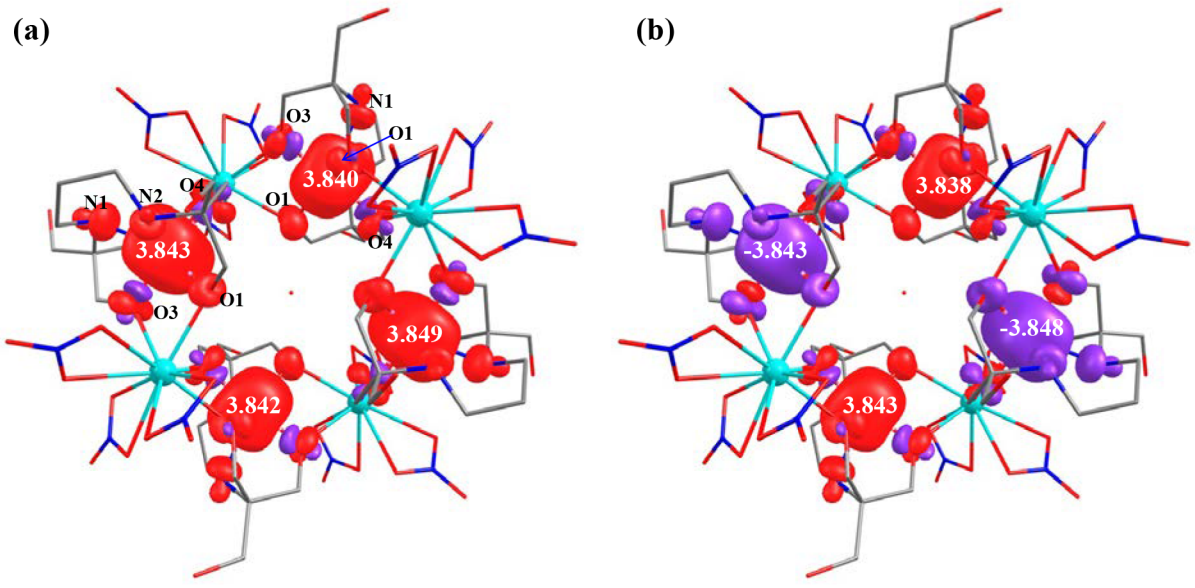

Figure 5. Computed spin density of the high-spin (HS) (a) and broken symmetry (BS) (b) states for complex **1** (hydrogen atoms are omitted for clarity).

DOI: 10.1021/acs.inorgchem.9b01592
Inorg. Chem. 2019, 58, 13815−13825

slow magnetic relaxation in mononuclear complexes containing Ce(III) and Nd(III),[81] and also in Mn(III)-Ln(III) complexes containing La(III) and Eu(III), albeit under applied dc fields.[82] However, for the compounds here, various applied fields in the range 100−5000 Oe did not lead to anything above negligible out-of-phase susceptibility; **1**−**4** therefore do not show any appreciable field induced slow relaxation.

Theoretical Study. To evaluate the magnetic properties of **1**, DFT and ab initio calculations were performed. To estimate the Mn(III)−Mn(III) exchange interaction, we have calculated the magnetic exchange for the full complex at the B3LYP/TZV level. Here, the magnetic exchange interaction between the two Mn(III) ions is mediated by the diamagnetic La(III) ion. This is the next-nearest neighbor interaction and is thus expected to be weak, but not negligible. In several instances of [3d-Ln-3d] compounds, relatively strong (1,3) 3d−3d interactions have been found.[83] Our DFT calculations yield a weak ferromagnetic exchange between the two Mn(III)centers with a J value estimated to be +0.15 cm^{-1}. This suggests that the Mn_4La_4 complex possesses an S = 8 ground state, arising from four high-spin Mn(III) ions.[78] To confirm the magnitude and sign of the J value computed, we simulated the magnetic susceptibility data and a very good fit to the experimental data is obtained, however a small intermolecular interaction (zJ = −0.03 cm^{-1}) is needed to reproduce the decrease in $\chi_M T$ at low temperature (see the SI, Figure S27) as we found when modeling the experimental data.

To probe the mechanism of the magnetic coupling, the spin density of both the high-spin (HS) and broken symmetry (BS) states was analyzed (see Figure 5). A qualitative mechanism of magnetic coupling for CuGd pairs, based on ab initio calculations, has been reported earlier.[84] All of the Mn(III) ions were found to possess a spin density of ∼3.8, suggesting slight delocalization of spin densities onto other coordinated atoms. This spin density pattern for Mn(III) promotes a mixture of spin delocalization and spin polarization, with the former prevailing on the longer Mn−O/N axes and the latter in the other directions. A closer look at the spin density reveals positive spin delocalization for the N1, N2, O1, and O2 atoms and negative spin delocalization for the O3 and O4 atoms (see Figure 5a for labels). The two oxygen atoms (O1 and O3) that bridge to the La(III) ion have both positive and negative spin densities, respectively. Overall, because spin delocalization is dominant, the La(III) ion is found to possess a small but positive residual spin density and this is due to the charge-transfer pathway between the Mn(III) ions and the empty 5*d*/6s/6p orbitals of the La(III) ion. This partial charge-transfer is facilitated because these formally empty orbitals lie relatively close in energy to the SOMOs of the Mn(III) ion, leading to net ferromagnetic coupling between the two Mn(III) ions (see Scheme 2 for an illustrative mechanism). This is due to the orthogonality between 3d and 4f orbitals and also to the charge transfer to empty 5d orbitals of the 4f ions.[85,86] Two possible mechanisms have been proposed in the literature where Ln(III) 4f orbitals are contracted around the nucleus and are efficiently shielded: (i) according to Kahn and co-workers, electron density can be transferred from the 3d orbitals of the M(III) ion to the empty 5d orbitals of the Ln(III) ion;[87,88] (ii) Gatteschi and co-workers suggested that a spin polarization mechanism is possible between the 3d orbitals of M(III) and the empty 6s orbital of the Ln(III) ion.[89,90] Both the mechanisms suggest the participation of 3d orbitals of M(III) and differ only with the involvement of empty Ln(III) orbitals

Scheme 2. Schematic Illustration of Magnetic Coupling between Two Mn(III) Ions via Diamagnetic La(III) Ions

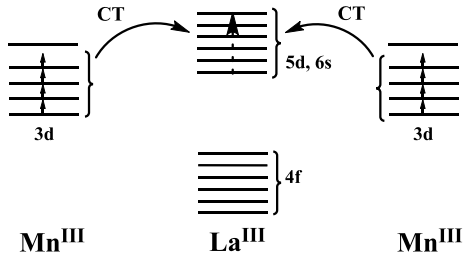

(6s or 5d).[84,91−94] CASSCF calculations on a Gd(III)−Cu(II) pair show that incorporation of the 5d orbital into the active space was necessary to reproduce the experimental J value and that the 5d orbitals of the Gd ion are responsible for the intrinsic ferromagnetic coupling.[95] Here one can expect a very similar behavior where 5d orbitals are likely to play a role in controlling the exchange interaction, perhaps more so than 6s/6p orbitals. However, detailed CASSCF calculations are needed to pinpoint the role of orbitals here as the structural topology and ligand framework are different. A qualitative mechanism is suggested based on earlier studies on various [3d-Ln-3d] systems where extensive analysis indicates the presence of a charge-transfer mechanism from 3d ions to the Ln(III) ions.[83,96] Additionally, the Mn(III)···Mn(III) distances are also relatively short (5.539(1) Å) suggesting an appreciable exchange coupling, as estimated from the DFT calculations. To further understand the mechanism of the exchange interaction, the overlap integrals between the SOMOs of the Mn(III) ions were computed (see SI Table S5). All the overlap integrals were found to be very small, which suggests orthogonality between the SOMOs, supporting the weak ferromagnetic coupling proposed.[97]

The nature of the magnetic anisotropy of the individual Mn(III) ions was evaluated using CASSCF calculations. For a single Mn(III) ion, the axial ZFS parameter D was found to be −2.85 cm^{-1} with E/D of 0.311 cm^{-1} at the CASSCF level, where E is the rhombic contribution to ZFS. Meanwhile, incorporation of a dynamic correlation via NEVPT2 yielded D = 3.155 cm^{-1} and E/D of 0.331 cm^{-1}. Although the sign of D is different for the two approaches, both yield E/D values that are very close to the rhombic limit (0.33 cm^{-1}), such that the sign of D cannot be unambiguously predicted from the calculations. To understand the electronic structure of the distorted Mn(III) ion, we analyzed the ground state wave function at the CASSCF level. The composition of the ground state was found to be 78% $(d_{yz})^1(d_{xz})^1(d_{xy})^1(d_{x^2-y^2})^1(d_{z^2})^0$ (see Figure 6) and 15% $(d_{yz})^1(d_{xz})^1(d_{xy})^1(d_{z^2})^1(d_{x^2-y^2})^0$, reflecting a mixture of configurations. However, the dominant configuration has the $d_{x^2-y^2}$ orbital lower in energy than the d_{z^2} orbital, and the d_{yz} orbital is found to be the lowest lying. The qualitative eigenvalue diagram derived from CASSCF orbitals/energies is shown in Figure 6. The strong angular distortion in the equatorial plane of the Mn(III) ion in **1** has three effects on the orbital ordering for the Mn(III) ion when compared to a regular Jahn−Teller environment.[98] First, it destabilizes the d_{xy} orbital because this orbital cannot participate in δ-type bonding at such a distorted angle due to d−p mixing; second, it stabilizes the $d_{x^2-y^2}$ orbital, because widened and acute angles reduce repulsion; and third, it lifts the degeneracy of the d_{xz} and d_{yz} orbitals.

DOI: 10.1021/acs.inorgchem.9b01592
Inorg. Chem. 2019, 58, 13815−13825

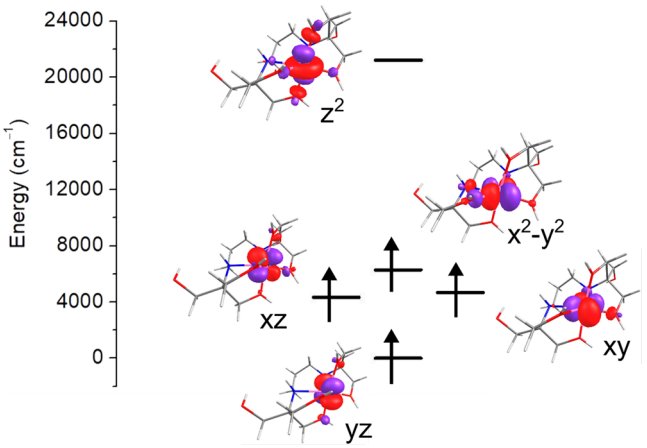

Figure 6. CASSCF computed metal-based d-orbitals for the ground state configuration at the isovalue of 0.03 e/Å^3 (see the text for details).

The axial ZFS of the Mn(III) ion is connected to the D(Ed$_{yz}$−Ed$_{z^2}$) gap and this gap is estimated to be 2.62 eV (Figure 6).[99] To fully understand the computed magnetic anisotropy, dominant contributions to the D and E/D values are shown in Table 2. At the NEVPT2 level (D = 3.155 cm^{-1}), the quintet states are found to contribute 0.87 cm^{-1} to the D value and a major contribution to this D value arises from the d$_{yz}$ → d$_{z^2}$ transition possessing different m_l values. The largest contribution to the net positive D value arises from the excited triplet states. Among the 35 triplets computed, the dominant contribution to the positive D arises from the lowest lying triplet state (1.526 cm^{-1}). This state has multiple contributions including a (d$_{yz}$)^1(d$_{xz}$)^2(d$_{xy}$)^1(d$_{x^2-y^2}$)^0(d$_{z^2}$)^0 triplet state where a d$_{x^2-y^2}$→ d$_{xz}$ spin-flip excitation was observed.

Table 2. Individual Contributions of the Energy States Contributing to the D Value of the Mn$_4$La$_4$ Complex (Only up to 12 Triplet Roots Are Shown)

states		NEVPT2 effective Hamiltonian approach		
		energy (cm^{-1})	contribution to D (cm^{-1})	contribution to E (cm^{-1})
^{5}D	^{5}A$_1$+	0	0	0
	^{5}A$_1$	8510.8	−0.028	−0.041
	^{5}B$_1$+	17 221	0.29	0.304
	^{5}B$_2$+	19 501.5	0.317	−0.139
	^{5}A$_2$	22 894.6	0.292	0.214
^{3}H	^{3}A$_2$+	9683.2	1.526	0.162
	^{3}B$_1$+	14 215.2	−0.264	0.099
	^{3}B$_2$+	15 898.3	0.589	0.12
	^{3}A$_1$+	20 200.3	−0.058	0.037
	^{3}B$_1$+	21 355.8	−0.106	0.213
	^{3}B$_2$	21 735.8	−0.082	−0.076
	^{3}A$_1$+	23 393.3	0.028	0.009
	^{3}A$_2$	24 358.3	0.084	0.006
	^{3}A$_1$+	25 084.3	−0.001	0.013
	^{3}B$_1$+	28 192.3	0.324	0.006
	^{3}B$_2$	29 184.3	0.353	0.013
			−0.121	−0.022
			overall	overall
			D = 3.155	E/D = 0.331

At the NEVPT2 level, a significant rhombic contribution to the magnetic anisotropy was found (E = 1.04 cm^{-1}) in addition to the axial ZFS. As seen for the contributions to D, the dominant contribution to E arises from the triplet spin states (the quintet spin states contribute 0.34 cm^{-1}). Among the triplet spin states, the largest contributory transition is the d$_{xy}$ → d$_{yz}$ transition. The lifting of the degeneracy of the d$_{xz}$ and d$_{yz}$ orbitals caused by the angular distortion around the Mn(III) ion leads to a large contribution to the E value and hence a large E/D value. This will increase quantum tunnelling of the magnetization and make the observation of slow magnetic relaxation unlikely, as was seen experimentally (see Figure S23). This is contrary to the report of a [Mn$_8$Y$_8$] wheel where out-of-phase signals in the ac susceptibility data were apparent even in the absence of a dc field.[78] In the Mn$_8$Y$_8$ case, the Mn(III) ions are clearly Jahn−Teller elongated with large negative D and small E/D values for the individual Mn(III) ions. In addition, the magnetic coupling is mediated by Y(III), and found to be larger (+0.45 cm^{-1}) than for **1**.

Optical Properties. The optical properties of **1**−**4** were investigated in the solid state using powder samples obtained from grinding crystals of the compounds, and the room temperature diffuse reflectance spectra are shown in Figure 7. Mn(III) has four 3d electrons and the ground state electronic configuration is largely (d$_{yz}$)^1(d$_{xz}$)^1(d$_{xy}$)^1(d$_{x^2-y^2}$)^1(d$_{z^2}$)^0 as explained in the previous section. Taking the low symmetry around the Mn(III) ion into account, up to four crystal field allowed transitions would be expected (see Table 2). However, the optical spectra consist of three broad absorption bands peaking at 430, 540, and 800 nm (23 255, 18 520, and 12 500 cm^{-1}, respectively). According to the theoretical study, all of the Mn(III) absorption spectra can be assigned to spin allowed d−d transitions of the Mn(III) ion in the high-spin configuration; namely from the ^{5}A$_1$ ground state to the ^{5}A$_1$, (^{5}B$_1$+^{5}B$_2$), and ^{5}A$_2$ excited states in approximate C_{2v} symmetry, although the actual symmetry of the Mn(III) ion is C_1. Despite the ^{5}A$_2$ ← ^{5}A$_1$ transition being forbidden in C_{2v} symmetry within electric dipole selection rules, this requirement can be relaxed for C_1 symmetry. The spectra for **1**−**3** only show broad features arising from the TM ion. Meanwhile, the reflectance spectrum measured for **4** shows weak sharp peaks at 583, 744, and 803 nm, which correspond to f−f intraconfigurational transitions of Nd(III) from the ground state, ^{4}I$_{9/2}$, to excited-state multiplets (^{4}G$_{5/2}$, ^{2}G$_{7/2}$), ^{4}F$_{7/2}$, and ^{4}F$_{5/2}$, respectively.

CONCLUSIONS AND OUTLOOK

Using the proligand H$_6$L, four polynuclear 3d-4f compounds have been prepared and characterized. Only the earliest members of the lanthanide series could be incorporated into the wheels, and the crystal structures of the complexes show the lanthanide ions to be decacoordinate in all four cases. This suggests that the later, smaller rare earth ions may be substituted by tuning the synthetic conditions to use monodentate anions rather than bidentate nitrate anions; this could lead to single-molecule toroic behavior, which has been reported for wheel-type Ln complexes.[100,101] The magnetic and theoretical study of the La-containing ring **1** showed that the magnetic exchange between the next-nearest neighbor TM ions is weak and ferromagnetic, and that the overall contribution of the distorted Mn(III) ions to the anisotropy of the ring is diminished because of the high E/D value. A potentially promising continuation of this work could therefore involve targeting the inclusion of Gd(III) ions in the rings, as a

DOI: 10.1021/acs.inorgchem.9b01592
Inorg. Chem. 2019, 58, 13815−13825

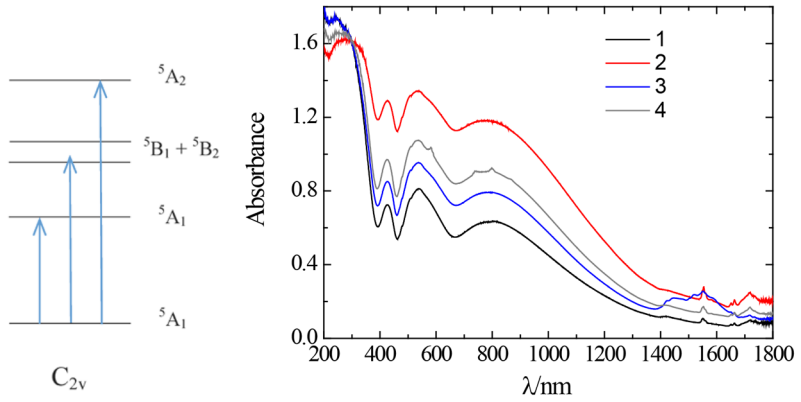

Figure 7. (Left) Energy level scheme for the MnO_4N_2 center. The electronic states are denoted by the symmetry labels corresponding to C_{2v} symmetry. Spin forbidden transitions have been omitted for the sake of clarity. The arrows represent observed transitions. (Right) Powder reflectance spectra for compounds **1**–**4**.

means of synthesizing mixed 3d-4f magnetic refrigerants.[102−104]

■ ASSOCIATED CONTENT

Supporting Information

The Supporting Information is available free of charge on the ACS Publications website at DOI: 10.1021/acs.inorgchem.9b01592.

PXRD patterns, TGA data, representative SEM-EDX measurements for each compound, continuous shape measurements for the Ln and Mn(III) ions, *M* vs *H* measurements and dynamic magnetic susceptibility study for all four compounds, additional tables detailing spin density, overlap integral values, and contributions to energy states (PDF)

Accession Codes

CCDC 1874195−1874198 contain the supplementary crystallographic data for this paper. These data can be obtained free of charge via www.ccdc.cam.ac.uk/data_request/cif, or by emailing data_request@ccdc.cam.ac.uk, or by contacting The Cambridge Crystallographic Data Centre, 12 Union Road, Cambridge CB2 1EZ, UK; fax: +44 1223 336033.

■ AUTHOR INFORMATION

Corresponding Authors

*E-mail: mark.murrie@glasgow.ac.uk.
*E-mail: rajaraman@chem.iitb.ac.in.

ORCID

Gavin A. Craig: 0000-0003-3542-4850
Rafael Valiente: 0000-0001-9855-8309
Gopalan Rajaraman: 0000-0001-6133-3026
Mark Murrie: 0000-0001-7297-2878

Present Address

[‖]Department of Pure and Applied Chemistry, University of Strathclyde, Glasgow, G1 1XL, United Kingdom

Notes

The authors declare no competing financial interest.

■ ACKNOWLEDGMENTS

The UK Engineering and Physical Sciences Research Council are thanked for financial support (Grant Ref EP/I027203/1, EP/K033662/1). Andy Monaghan and Jim Gallagher (University of Glasgow) are thanked for running TGA measurements and the SEM-EDX experiments, respectively. Olivier Roubeau (University of Zaragoza) is thanked for carrying out the magnetic measurements on compound **4**. We thank the EPSRC UK National Crystallography Service at the University of Southampton for collection of the crystallographic data. G.V. would like to thank the Indian Institute of Technology Bombay for a Post-Doctoral fellowship. G.R. would like to thank SERB (CRG/2018/000430) and UGC-UKIERI (184-1/2018(IC)) for funding. MINECO under Project MAT2015-69508-P is also acknowledged (R.V.).

■ REFERENCES

(1) Meng, Y.-S.; Jiang, S.-D.; Wang, B.-W.; Gao, S. Understanding the Magnetic Anisotropy Toward Single-Ion Magnets. *Acc. Chem. Res.* **2016**, *49*, 2381−2389.

(2) Craig, G. A.; Murrie, M. 3d Single-ion Magnets. *Chem. Soc. Rev.* **2015**, *44*, 2135−2147.

(3) Gómez-Coca, S.; Aravena, D.; Morales, R.; Ruiz, E. Large Magnetic Anistropy in Mononuclear Metal Complexes. *Coord. Chem. Rev.* **2015**, *289*−*290*, 379−392.

(4) Sun, H.-L.; Wang, Z.-M.; Gao, S. Strategies Towards Single-chain Magnets. *Coord. Chem. Rev.* **2010**, *254*, 1081−1100.

(5) Roubeau, O.; Clérac, R. Rational Assembly of High-Spin Polynuclear Magnetic Complexes into Coordination Networks: the Case of a [Mn_4] Single-Molecule Magnet Building Block. *Eur. J. Inorg. Chem.* **2008**, *2008*, 4325−4342.

(6) Xu, H.-B.; Wang, B.-W.; Pan, F.; Wang, Z.-M.; Gao, S. Stringing Oxo-Centered Trinuclear [Mn_3O] Units into Single-Chain Magnets with Formate or Azide Linkers. *Angew. Chem.* **2007**, *119*, 7532−7536.

(7) Fataftah, M. S.; Coste, S. C.; Vlaisavljevich, B.; Zadrozny, J. M.; Freedman, D. E. Transformation of the Coordination Complex $[Co(C_3S_5)^2]^{2-}$ from a Molecular Magnet to a Potential Qubit. *Chem. Sci.* **2016**, *7*, 6160−6166.

(8) Aguilà, D.; Barrios, L. A.; Velasco, V.; Roubeau, O.; Repollés, A.; Alonso, P. J.; Sesé, J.; Teat, S. J.; Luis, F.; Aromí, G. Heterodimetallic [LnLn'] Lanthanide Complexes: Toward a Chemical Design of Two-Qubit Molecular Spin Quantum Gates. *J. Am. Chem. Soc.* **2014**, *136*, 14215−14222.

(9) Bader, K.; Dengler, D.; Lenz, S.; Endeward, B.; Jiang, S. D.; Neugebauer, P.; van Slageren, J. Room Temperature Quantum Coherence in a Potential Molecular Qubit. *Nat. Commun.* **2014**, *5*, 5304.

(10) Baldoví, J. J.; Cardona-Serra, S.; Clemente-Juan, J. M.; Coronado, E.; Gaita-Ariño, A.; Palii, A. Rational Design of Single-Ion Magnets and Spin Qubits Based on Mononuclear Lanthanoid Complexes. *Inorg. Chem.* **2012**, *51*, 12565−12574.

DOI: 10.1021/acs.inorgchem.9b01592
Inorg. Chem. 2019, 58, 13815−13825

(11) Gatteschi, D.; Sessoli, R.; Villain, J. Molecular Nanomagnets. *In Molecular Nanomagnets; Mesoscopic Physics and Nanotechnology* **2006**, 1−395.
(12) Rosado Piquer, L.; Sañudo, E. C. Heterometallic 3d-4f Single-molecule Magnets. *Dalton Trans* **2015**, *44*, 8771−8780.
(13) Liu, K.; Shi, W.; Cheng, P. Toward Heterometallic Single-molecule Magnets: Synthetic Strategy, Structures and Properties of 3d-4f Discrete Complexes. *Coord. Chem. Rev.* **2015**, *289*−*290*, 74−122.
(14) Liddle, S. T.; van Slageren, J. Improving f-element Single Molecule Magnets. *Chem. Soc. Rev.* **2015**, *44*, 6655−6669.
(15) Chilton, N. F. Design Criteria for High-Temperature Single-Molecule Magnets. *Inorg. Chem.* **2015**, *54*, 2097−2099.
(16) Ojea, M. J. H.; Lorusso, G.; Craig, G. A.; Wilson, C.; Evangelisti, M.; Murrie, M. A topologically unique alternating [CoIII3GdIII3] magnetocaloric ring. *Chem. Commun.* **2017**, *53*, 4799−4802.
(17) Rajeshkumar, T.; Annadata, H. V.; Evangelisti, M.; Langley, S. K.; Chilton, N. F.; Murray, K. S.; Rajaraman, G. Theoretical Studies on Polynuclear $[Cu(II)_5Gd(III)_n]$ Clusters (n = 4, 2): Towards Understanding Their Large Magnetocaloric Effect. *Inorg. Chem.* **2015**, *54*, 1661−1670.
(18) Zheng, Y.-Z.; Zhou, G.-J.; Zheng, Z.; Winpenny, R. E. P. Molecule-based Magnetic Coolers. *Chem. Soc. Rev.* **2014**, *43*, 1462−1475.
(19) Kettles, F. J.; Milway, V. A.; Tuna, F.; Valiente, R.; Thomas, L. H.; Wernsdorfer, W.; Ochsenbein, S. T.; Murrie, M. Exchange Interactions at the Origin of Slow Relaxation of the Magnetization in $[TbCu_3]$ and $[DyCu_3]$ Single-Molecule Magnets. *Inorg. Chem.* **2014**, *53*, 8970−8978.
(20) Okazawa, A.; Shimada, T.; Kojima, N.; Yoshii, S.; Nojiri, H.; Ishida, T. Exchange Coupling and Its Chemical Trend Studied by High-Frequency EPR on Heterometallic $[Ln_2Ni]$ Complexes. *Inorg. Chem.* **2013**, *52*, 13351−13355.
(21) Schray, D.; Abbas, G.; Lan, Y.; Mereacre, V.; Sundt, A.; Dreiser, J.; Waldmann, O.; Kostakis, G. E.; Anson, C. E.; Powell, A. K. Combined Magnetic Susceptibility Measurements and ^{57}Fe Mössbauer Spectroscopy on a Ferromagnetic $[Fe(III)_4Dy_4]$ Ring. *Angew. Chem., Int. Ed.* **2010**, *49*, 5185−5188.
(22) Moreno Pineda, E.; Chilton, N. F.; Tuna, F.; Winpenny, R. E. P.; McInnes, E. J. L. Systematic Study of a Family of Butterfly-Like $[M_2Ln_2]$ Molecular Magnets (M = Mg(II), Mn(III), Co(II), Ni(II), and Cu(II); Ln = Y(III), Gd(III), Tb(III), Dy(III), Ho(III), and Er(III)). *Inorg. Chem.* **2015**, *54*, 5930−5941.
(23) Tziotzi, T. G.; Kalofolias, D. A.; Tzimopoulos, D. I.; Siczek, M.; Lis, T.; Inglis, R.; Milios, C. J. A Family of $[Mn(III)_6Ln(III)_2]$ Rod-like Clusters. *Dalton Trans* **2015**, *44*, 6082−6088.
(24) Cao, F.; Wang, S.; Li, D.; Zeng, S.; Niu, M.; Song, Y.; Dou, J. Family of Mixed 3d-4f Dimeric 14-Metallacrown-5 Compounds: Syntheses, Structures, and Magnetic Properties. *Inorg. Chem.* **2013**, *52*, 10747−10755.
(25) Polyzou, C. D.; Nikolaou, H.; Papatriantafyllopoulou, C.; Psycharis, V.; Terzis, A.; Raptopoulou, C. P.; Escuer, A.; Perlepes, S. P. Employment of Methyl 2-pyridyl Ketone Oxime in 3d/4f-metal Chemistry: Dinuclear Nickel(II)/Lanthanide(III) Species and Complexes Containing the Metals in Separate Ions. *Dalton Trans* **2012**, *41*, 13755−13764.
(26) Li, M.; Lan, Y.; Ako, A. M.; Wernsdorfer, W.; Anson, C. E.; Buth, G.; Powell, A. K.; Wang, Z.; Gao, S. A Family of 3d-4f Octa-Nuclear $[Mn(III)_4Ln(III)_4]$ Wheels (Ln = Sm, Gd, Tb, Dy, Ho, Er, and Y): Synthesis, Structure, and Magnetism. *Inorg. Chem.* **2010**, *49*, 11587−11594.
(27) Ako, A. M.; Mereacre, V.; Clérac, R.; Hewitt, I. J.; Lan, Y.; Buth, G.; Anson, C. E.; Powell, A. K. Tridecanuclear $[Mn(III)_5Ln(III)_8]$ Complexes Derived from N-^{t}Butyl-diethanolamine: Synthesis, Structures, and Magnetic Properties. *Inorg. Chem.* **2009**, *48*, 6713−6723.
(28) Estrader, M.; Ribas, J.; Tangoulis, V.; Solans, X.; Font-Bardía, M.; Maestro, M.; Diaz, C. Synthesis, Crystal Structure, and Magnetic Studies of One-Dimensional Cyano-Bridged Ln(III)-Cr(III) Complexes with bpy as a Blocking Ligand. *Inorg. Chem.* **2006**, *45*, 8239−8250.
(29) Ledezma-Gairaud, M.; Grangel, L.; Aromí, G.; Fujisawa, T.; Yamaguchi, A.; Sumiyama, A.; Sañudo, E. C. From Serendipitous Assembly to Controlled Synthesis of 3d-4f Single-Molecule Magnets. *Inorg. Chem.* **2014**, *53*, 5878−5880.
(30) Ako, A. M.; Mereacre, V.; Clerac, R.; Wernsdorfer, W.; Hewitt, I. J.; Anson, C. E.; Powell, A. K. A $[Mn_{18}Dy]$ SMM Resulting from the Targeted Replacement of the Central Mn(II) in the S = 83/2 $[Mn_{19}]$-Aggregate with Dy(III). *Chem. Commun.* **2009**, 544−546.
(31) Sharples, J. W.; Collison, D. The Coordination Chemistry and Magnetism of Some 3d-4f and 4f Amino-polyalcohol Compounds. *Coord. Chem. Rev.* **2014**, *260*, 1−20.
(32) Heras Ojea, M. J.; Wilson, C.; Coles, S. J.; Tuna, F.; Murrie, M. Directed Synthesis of $[Cu(II)_2Zn(II)_2]$ and $[Cu(II)_8Zn(II)_8]$ Heterometallic Complexes. *Dalton Trans* **2015**, *44*, 19275−19281.
(33) Milway, V. A.; Tuna, F.; Farrell, A. R.; Sharp, L. E.; Parsons, S.; Murrie, M. Directed Synthesis of $[Mn_{18}Cu_6]$ Heterometallic Complexes. *Angew. Chem., Int. Ed.* **2013**, *52*, 1949−1952.
(34) Ferguson, A.; Schmidtmann, M.; Brechin, E. K.; Murrie, M. Bis-tris Propane as a New Multidentate Ligand for Nickel- and Cobalt-based Spin Clusters. *Dalton Trans* **2011**, *40*, 334−336.
(35) Ferguson, A.; Darwish, A.; Graham, K.; Schmidtmann, M.; Parkin, A.; Murrie, M. Bis-Tris Propane as a New Polydentate Linker in the Synthesis of Iron(III) and Manganese(II/III) Complexes. *Inorg. Chem.* **2008**, *47*, 9742−9744.
(36) Murrie, M. Bis-tris propane as a flexible ligand for high-nuclearity complexes. *Polyhedron* **2018**, *150*, 1−9.
(37) Heras Ojea, M. J.; Milway, V. A.; Velmurugan, G.; Thomas, L. H.; Coles, S. J.; Wilson, C.; Wernsdorfer, W.; Rajaraman, G.; Murrie, M. Enhancement of Tb(III)-Cu(II) Single-Molecule Magnet Performance through Structural Modification. *Chem. - Eur. J.* **2016**, *22*, 12839−12848.
(38) Coles, S. J.; Gale, P. A. Changing and Challenging Times for Service Crystallography. *Chem. Sci.* **2012**, *3*, 683−689.
(39) Palatinus, L.; Chapuis, G. Superflip. *J. Appl. Crystallogr.* **2007**, *40*, 786−790.
(40) Betteridge, P. W.; Carruthers, J. R.; Cooper, R. I.; Prout, K.; Watkin, D. J. CRYSTALS. *J. Appl. Crystallogr.* **2003**, *36*, 1487.
(41) Dolomanov, O. V.; Bourhis, L. J.; Gildea, R. J.; Howard, J. A. K.; Puschmann, H. OLEX2: a complete structure solution, refinement and analysis program. *J. Appl. Crystallogr.* **2009**, *42*, 339−341.
(42) Sheldrick, G. Crystal structure refinement with SHELXL. *Acta Crystallogr., Sect. C: Struct. Chem.* **2015**, *C71*, 3−8.
(43) Sheldrick, G. A short history of SHELX. *Acta Crystallogr., Sect. A: Found. Crystallogr.* **2008**, *A64*, 112−122.
(44) Macrae, C. F.; Bruno, I. J.; Chisholm, J. A.; Edgington, P. R.; McCabe, P.; Pidcock, E.; Rodríguez-Monge, L.; Taylor, R.; van de Streek, J.; Wood, P. A. Mercury CSD 2.0 - New Features for the Visualization and Investigation of Crystal Structures. *J. Appl. Crystallogr.* **2008**, *41*, 466−470.
(45) Frisch, M. J.; Trucks, G. W.; Schlegel, H. B.; Scuseria, G. E.; Robb, M. A.; Cheeseman, J. R.; Scalmani, G.; Barone, V.; Mennucci, B.; Petersson, G. A.; Nakatsuji, H.; Caricato, M.; Li, X.; Hratchian, H. P.; Izmaylov, A. F.; Bloino, J.; Zheng, G.; Sonnenberg, J. L.; Hada, M.; Ehara, M.; Toyota, K.; Fukuda, R.; Hasegawa, J.; Ishida, M.; Nakajima, T.; Honda, Y.; Kitao, O.; Nakai, H.; Vreven, T.; J. A. Montgomery, J.; Peralta, J. E.; Ogliaro, F.; Bearpark, M.; Heyd, J. J.; Brothers, E.; Kudin, K. N.; Staroverov, V. N.; Kobayashi, R.; Normand, J.; Raghavachari, K.; Rendell, A.; Burant, J. C.; Iyengar, S. S.; Tomasi, J.; Cossi, M.; Rega, N.; Millam, J. M.; Klene, M.; Knox, J. E.; Cross, J. B.; Bakken, V.; Adamo, C.; Jaramillo, J.; Gomperts, R.; Stratmann, R. E.; Yazyev, O.; Austin, A. J.; Cammi, R.; Pomelli, C.; Ochterski, J. W.; Martin, R. L.; Morokuma, K.; Zakrzewski, V. G.; Voth, G. A.; Salvador, P.; Dannenberg, J. J.; Dapprich, S.; Daniels, A. D.; Farkas, Ö.; Foresman, J. B.; Ortiz, J. V.; Cioslowski, J.; Fox, D. J. *Gaussian09*; Gaussian, Inc.: Wallingford CT. 2009.
(46) Becke, A. D. Density-Functional Thermochemistry 3. The Role of Exact Exchange. *J. Chem. Phys.* **1993**, *98*, 5648−5652.

DOI: 10.1021/acs.inorgchem.9b01592
Inorg. Chem. 2019, 58, 13815−13825

(47) Schafer, A.; Huber, C.; Ahlrichs, R. Fully Optimized Contracted Gaussian-Basis Sets of Triple Zeta Valence Quality for Atoms Li to Kr. *J. Chem. Phys.* **1994**, *100*, 5829−5835.
(48) Schafer, A.; Horn, H.; Ahlrichs, R. Fully Optimized Contracted Gaussian-basis Sets for Atoms Li to Kr. *J. Chem. Phys.* **1992**, *97*, 2571−2577.
(49) Noodleman, L. Valence Bond Description of Anti-Ferromagnetic Coupling in Transition-Metal Dimers. *J. Chem. Phys.* **1981**, *74*, 5737−5743.
(50) Bencini, A.; Totti, F. DFT description of the magnetic structure of polynuclear transition-metal clusters: The complexes $[(Cu(bpca)_2(H_2O)_2)(Cu(NO_3)_2)_2]$, (bpca = Bis(2-pyridylcarbonyl)-amine), and $[Cu(DBSQ)(C_2H_5O)]_2$, (DBSQ = 3,5-di-tert-butyl-semiquinonato). *Int. J. Quantum Chem.* **2005**, *101*, 819−825.
(51) Christian, P.; Rajaraman, G.; Harrison, A.; Helliwell, M.; McDouall, J. J. W.; Raftery, J.; Winpenny, R. E. P. Synthesis and studies of a trinuclear Mn(II) carboxylate complex. *Dalton Trans* **2004**, 2550−2555.
(52) Hegetschweiler, K.; Morgenstern, B.; Zubieta, J.; Hagrman, P. J.; Lima, N.; Sessoli, R.; Totti, F. Strong Ferromagnetic Interactions in $[V_8O_{14}(H\text{-}2taci)_2]$: An Unprecedented Large Spin Ground State for a Vanadyl Cluster. *Angew. Chem., Int. Ed.* **2004**, *43*, 3436−3439.
(53) Rajaraman, G.; Cano, J.; Brechin, E. K.; McInnes, E. J. L. Density functional calculations of a tetradecametallic iron(III) cluster with a very large spin ground state. *Chem. Commun.* **2004**, 1476−1477.
(54) Rajaraman, G.; Murugesu, M.; Sañudo, E. C.; Soler, M.; Wernsdorfer, W.; Helliwell, M.; Muryn, C.; Raftery, J.; Teat, S. J.; Christou, G.; Brechin, E. K. A Family of Manganese Rods: Syntheses, Structures, and Magnetic Properties. *J. Am. Chem. Soc.* **2004**, *126*, 15445−15457.
(55) Ruiz, E.; Cano, J.; Alvarez, S.; Caneschi, A.; Gatteschi, D. Theoretical Study of the Magnetic Behavior of Hexanuclear Cu(II) and Ni(II) Polysiloxanolato Complexes. *J. Am. Chem. Soc.* **2003**, *125*, 6791−6794.
(56) Ruiz, E.; Rodríguez-Fortea, A.; Cano, J.; Alvarez, S.; Alemany, P. About the calculation of exchange coupling constants in polynuclear transition metal complexes. *J. Comput. Chem.* **2003**, *24*, 982−989.
(57) Ruiz, E.; Cano, J.; Alvarez, S.; Alemany, P. Broken symmetry approach to calculation of exchange coupling constants for homobinuclear and heterobinuclear transition metal complexes. *J. Comput. Chem.* **1999**, *20*, 1391−1400.
(58) Comar, P.; Rajeshkumar, T.; Nichol, G. S.; Pitak, M. B.; Coles, S. J.; Rajaraman, G.; Brechin, E. K. Switching the Orientation of Jahn-Teller Axes in Oxime-based Mn(III) Dimers and its Effect Upon Magnetic Exchange: A Combined Experimental and Theoretical Study. *Dalton Trans* **2015**, *44*, 19805−19811.
(59) Barros, W. P.; Inglis, R.; Nichol, G. S.; Rajeshkumar, T.; Rajaraman, G.; Piligkos, S.; Stumpf, H. O.; Brechin, E. K. From Antiferromagnetic to Ferromagnetic Exchange in a Family of Oxime-based Mn(III) Dimers: A Magneto-structural Study. *Dalton Trans* **2013**, *42*, 16510−16517.
(60) Berg, N.; Rajeshkumar, T.; Taylor, S. M.; Brechin, E. K.; Rajaraman, G.; Jones, L. F. What Controls the Magnetic Interaction in bis-;-Alkoxo Mn(III) Dimers? A Combined Experimental and Theoretical Exploration. *Chem. - Eur. J.* **2012**, *18*, 5906−5918.
(61) Gupta, T.; Rajeshkumar, T.; Rajaraman, G. Magnetic exchange in [Gd^{III}-radical] complexes: method assessment, mechanism of coupling and magneto-structural correlations. *Phys. Chem. Chem. Phys.* **2014**, *16*, 14568−14577.
(62) Neese, F. The ORCA Program System. *WIREs Comput. Mol. Sci.* **2012**, *2*, 73−78.
(63) Angeli, C.; Cimiraglia, R.; Malrieu, J.-P. n-electron valence state perturbation theory: A spinless formulation and an efficient implementation of the strongly contracted and of the partially contracted variants. *J. Chem. Phys.* **2002**, *117*, 9138−9153.
(64) Angeli, C.; Cimiraglia, R.; Evangelisti, S.; Leininger, T.; Malrieu, J. P. Introduction of n-electron valence states for multi-reference perturbation theory. *J. Chem. Phys.* **2001**, *114*, 10252−10264.
(65) Angeli, C.; Cimiraglia, R.; Malrieu, J.-P. N-electron valence state perturbation theory: a fast implementation of the strongly contracted variant. *Chem. Phys. Lett.* **2001**, *350*, 297−305.
(66) Maurice, R.; Bastardis, R.; Graaf, C. d.; Suaud, N.; Mallah, T.; Guihéry, N. Universal Theoretical Approach to Extract Anisotropic Spin Hamiltonians. *J. Chem. Theory Comput.* **2009**, *5*, 2977−2984.
(67) Ganyushin, D.; Neese, F. First-principles calculations of zero-field splitting parameters. *J. Chem. Phys.* **2006**, *125*, 024103.
(68) Pierloot, K.; Phung, Q. M.; Domingo, A. Spin State Energetics in First-Row Transition Metal Complexes: Contribution of (3s3p) Correlation and Its Description by Second-Order Perturbation Theory. *J. Chem. Theory Comput.* **2017**, *13*, 537−553.
(69) Sivalingam, K.; Krupicka, M.; Auer, A. A.; Neese, F. Comparison of fully internally and strongly contracted multireference configuration interaction procedures. *J. Chem. Phys.* **2016**, *145*, 054104.
(70) Mereacre, V.; Lan, Y.; Clérac, R.; Ako, A. M.; Wernsdorfer, W.; Buth, G.; Anson, C. E.; Powell, A. K. Contribution of Spin and Anisotropy to Single Molecule Magnet Behavior in a Family of Bell-Shaped $Mn_{11}Ln_2$Coordination Clusters. *Inorg. Chem.* **2011**, *50*, 12001−12009.
(71) Spek, A. L. PLATON. *Acta Crystallogr., Sect. D: Biol. Crystallogr.* **2009**, *D65*, 148−155.
(72) Aguilà, D.; Barrios, L. A.; Velasco, V.; Arnedo, L.; Aliaga-Alcalde, N.; Menelaou, M.; Teat, S. J.; Roubeau, O.; Luis, F.; Aromí, G. Lanthanide Contraction within a Series of Asymmetric Dinuclear $[Ln_2]$ Complexes. *Chem. - Eur. J.* **2013**, *19*, 5881−5891.
(73) Li, M.; Ako, A. M.; Lan, Y.; Wernsdorfer, W.; Buth, G.; Anson, C. E.; Powell, A. K.; Wang, Z.; Gao, S. New Heterometallic $[Mn(III)_4Ln(III)_4]$ Wheels Incorporating Formate Ligands. *Dalton Trans* **2010**, *39*, 3375−3377.
(74) Chilton, N. F.; Anderson, R. P.; Turner, L. D.; Soncini, A.; Murray, K. S. PHI: A Powerful New Program for the Analysis of Anisotropic Monomeric and Exchange-coupled Polynuclear d- and f-Block Complexes. *J. Comput. Chem.* **2013**, *34*, 1164−1175.
(75) Yang, H.; Cao, F.; Li, D.; Zeng, S.; Song, Y.; Dou, J. A Family of 12-Azametallacrown-4 Structural Motif with Heterometallic Mn^{III}-Ln-Mn^{III}-Ln (Ln = Dy, Er, Yb, Tb, Y) Alternate Arrangement and Single-Molecule Magnet Behavior. *Chem. - Eur. J.* **2015**, *21*, 14478−14485.
(76) Ako, A. M.; Burger, B.; Lan, Y.; Mereacre, V.; Clérac, R.; Buth, G.; Gómez-Coca, S.; Ruiz, E.; Anson, C. E.; Powell, A. K. Magnetic Interactions Mediated by Diamagnetic Cations in $[Mn_{18}M]$ (M = Sr^{2+}, Y^{3+}, Cd^{2+}, and Lu^{3+}) Coordination Clusters. *Inorg. Chem.* **2013**, *52*, 5764−5774.
(77) Liu, J.; Ma, C.; Chen, H.; Hu, M.; Wen, H.; Cui, H.; Chen, C. The First Heterometallic Examples of 3d-4f Heptanuclear $[Mn(II)_3Ln(III)_4]$ Complexes with Planar Disc-like Cores and Diverse Magnetic Properties. *Dalton Trans* **2013**, *42*, 3787−3790.
(78) Vignesh, K. R.; Langley, S. K.; Moubaraki, B.; Murray, K. S.; Rajaraman, G. Large Hexadecametallic [Mn(III)-Ln(III)] Wheels: Synthesis, Structural, Magnetic, and Theoretical Characterization. *Chem. - Eur. J.* **2015**, *21*, 16364−16369.
(79) Ahmed, N.; Das, C.; Vaidya, S.; Srivastava, A. K.; Langley, S. K.; Murray, K. S.; Shanmugam, M. Probing the Magnetic and Magnetothermal Properties of M(II)-Ln(III) Complexes (where M(II) = Ni or Zn; Ln(III) = La or Pr or Gd). *Dalton Trans* **2014**, *43*, 17375−17384.
(80) Baniodeh, A.; Magnani, N.; Lan, Y.; Buth, G.; Anson, C. E.; Richter, J.; Affronte, M.; Schnack, J.; Powell, A. K. High spin cycles: topping the spin record for a single molecule verging on quantum criticality. *npj Quantum Mater.* **2018**, *3*, 10.
(81) Wada, H.; Ooka, S.; Yamamura, T.; Kajiwara, T. Light Lanthanide Complexes with Crown Ether and Its Aza Derivative Which Show Slow Magnetic Relaxation Behaviors. *Inorg. Chem.* **2017**, *56*, 147−155.
(82) Escobar, L. B. L.; Guedes, G. P.; Soriano, S.; Cassaro, R. A. A.; Marbey, J.; Hill, S.; Novak, M. A.; Andruh, M.; Vaz, M. G. F.

DOI: 10.1021/acs.inorgchem.9b01592
Inorg. Chem. 2019, 58, 13815−13825

Synthesis, Crystal Structures, and EPR Studies of First MnIIILnIII Hetero-binuclear Complexes. *Inorg. Chem.* **2018**, *57*, 326−334.
(83) Singh, S. K.; Tibrewal, N. K.; Rajaraman, G. Density Functional Studies on Dinuclear [(Ni(II)Gd(III)] and Trinuclear [(Ni(II)Gd-(III)Ni(II))] Complexes: Magnetic Exchange and Magneto-structural Maps. *Dalton Trans* **2011**, *40*, 10897−10906.
(84) Paulovič, J.; Cimpoesu, F.; Ferbinteanu, M.; Hirao, K. Mechanism of Ferromagnetic Coupling in Copper(II)-Gadolinium-(III) Complexes. *J. Am. Chem. Soc.* **2004**, *126*, 3321−3331.
(85) Singh, S. K.; Rajaraman, G. Decisive interactions that determine ferro/antiferromagnetic coupling in [3d-4f] pairs: a case study on dinuclear [V(IV)-Gd(III)] complexes. *Dalton Trans* **2013**, *42*, 3623−3630.
(86) Sweet, L. E.; Roy, L. E.; Meng, F.; Hughbanks, T. Ferromagnetic Coupling in Hexanuclear Gadolinium Clusters. *J. Am. Chem. Soc.* **2006**, *128*, 10193−10201.
(87) Ramade, I.; Kahn, O.; Jeannin, Y.; Robert, F. Design and Magnetic Properties of a Magnetically Isolated GdIIICuII Pair. Crystal Structures of $[Gd(hfa)_3Cu(salen)]$, $[Y(hfa)_3Cu(salen)]$, $[Gd(hfa)_3Cu(salen)(Meim)]$, and $[La(hfa)_3(H_2O)Cu(salen)]$ [hfa = Hexafluoroacetylacetonato, salen = N,N′-Ethylenebis-(salicylideneaminato), Meim = 1-Methylimidazole]. *Inorg. Chem.* **1997**, *36*, 930−936.
(88) Andruh, M.; Ramade, I.; Codjovi, E.; Guillou, O.; Kahn, O.; Trombe, J. C. Crystal structure and magnetic properties of $[Ln_2Cu_4]$ hexanuclear clusters (where Ln = trivalent lanthanide). Mechanism of the gadolinium(III)-copper(II) magnetic interaction. *J. Am. Chem. Soc.* **1993**, *115*, 1822−1829.
(89) Benelli, C.; Caneschi, A.; Gatteschi, D.; Sessoli, R. Magnetic properties and phase transitions in molecular based materials containing rare earth ions and organic radicals. *J. Appl. Phys.* **1993**, *73*, 5333−5337.
(90) Benelli, C.; Caneschi, A.; Gatteschi, D.; Guillou, O.; Pardi, L. Synthesis, crystal structure, and magnetic properties of tetranuclear complexes containing exchange-coupled dilanthanide-dicopper-(lanthanide = gadolinium, dysprosium) species. *Inorg. Chem.* **1990**, *29*, 1750−1755.
(91) Feltham, H. L. C.; Dumas, C.; Mannini, M.; Otero, E.; Sainctavit, P.; Sessoli, R.; Meledandri, C. J.; Brooker, S. Proof of Principle: Immobilisation of Robust $Cu^{II}_3Tb^{III}$-Macrocycles on Small, Suitably Pre-functionalised Gold Nanoparticles. *Chem. - Eur. J.* **2017**, *23*, 2517−2521.
(92) Cremades, E.; Gómez-Coca, S.; Aravena, D.; Alvarez, S.; Ruiz, E. Theoretical Study of Exchange Coupling in 3d-Gd Complexes: Large Magnetocaloric Effect Systems. *J. Am. Chem. Soc.* **2012**, *134*, 10532−10542.
(93) Pointillart, F.; Bernot, K.; Poneti, G.; Sessoli, R. Crystal Packing Effects on the Magnetic Slow Relaxation of Tb(III)-Nitronyl Nitroxide Radical Cyclic Dinuclear Clusters. *Inorg. Chem.* **2012**, *51*, 12218−12229.
(94) Pasatoiu, T. D.; Etienne, M.; Madalan, A. M.; Andruh, M.; Sessoli, R. Dimers and chains of {3d-4f} single molecule magnets constructed from heterobimetallic tectons. *Dalton Trans* **2010**, *39*, 4802−4808.
(95) Rajaraman, G.; Totti, F.; Bencini, A.; Caneschi, A.; Sessoli, R.; Gatteschi, D. Density functional studies on the exchange interaction of a dinuclear Gd(III)-Cu(II) complex: method assessment, magnetic coupling mechanism and magneto-structural correlations. *Dalton Trans* **2009**, 3153−3161.
(96) Ghosh, S.; Singh, S. K.; Tewary, S.; Rajaraman, G. Enhancing the double exchange interaction in a mixed valence $[V^{III}$-$V^{II}]$ pair: a theoretical perspective. *Dalton Trans* **2013**, *42*, 16490−16493.
(97) Frost, J. M.; Sanz, S.; Rajeshkumar, T.; Pitak, M. B.; Coles, S. J.; Rajaraman, G.; Wernsdorfer, W.; Schnack, J.; Lusby, P. J.; Brechin, E. K. A truncated $Mn(III)_{12}$ Tetrahedron from Oxime-based $[Mn(III)_3O]$ Building Blocks. *Dalton Trans* **2014**, *43*, 10690−10694.
(98) Singh, S. K.; Gupta, T.; Badkur, P.; Rajaraman, G. Magnetic Anisotropy of Mononuclear Ni(II) Complexes: On the Importance of Structural Diversity and the Structural Distortions. *Chem. - Eur. J.* **2014**, *20*, 10305−10313.
(99) Berg, N.; Hooper, T. N.; Liu, J. J.; Beedle, C. C.; Singh, S. K.; Rajaraman, G.; Piligkos, S.; Hill, S.; Brechin, E. K.; Jones, L. F. Synthetic, Structural, Spectroscopic and Theoretical Study of a Mn(III)-Cu(II) Dimer Containing a Jahn-Teller Compressed Mn Ion. *Dalton Trans* **2013**, *42*, 207−216.
(100) Langley, S. K.; Vignesh, K. R.; Moubaraki, B.; Rajaraman, G.; Murray, K. S. Oblate versus Prolate Electron Density of Lanthanide Ions: A Design Criterion for Engineering Toroidal Moments? A Case Study on $[Ln^{III}_6]$ (Ln = Tb, Dy, Ho and Er) Wheels. *Chem. - Eur. J.* **2019**, *25*, 4156−4165.
(101) Wu, J.; Li, X.-L.; Guo, M.; Zhao, L.; Zhang, Y.-Q.; Tang, J. Realization of toroidal magnetic moments in heterometallic 3d-4f metallocycles. *Chem. Commun.* **2018**, *54*, 1065−1068.
(102) Liu, J.-L.; Lin, W.-Q.; Chen, Y.-C.; Leng, J.-D.; Guo, F.-S.; Tong, M.-L. Symmetry-Related $[Ln_6Mn_{12}]$ Clusters toward Single-Molecule Magnets and Cryogenic Magnetic Refrigerants. *Inorg. Chem.* **2013**, *52*, 457−463.
(103) Sharples, J. W.; Collison, D. Coordination Compounds and the Magnetocaloric Effect. *Polyhedron* **2013**, *54*, 91−103.
(104) Karotsis, G.; Kennedy, S.; Teat, S. J.; Beavers, C. M.; Fowler, D. A.; Morales, J. J.; Evangelisti, M.; Dalgarno, S. J.; Brechin, E. K. $[Mn_4Ln_4]$ Calix[4]arene Clusters as Enhanced Magnetic Coolers and Molecular Magnets. *J. Am. Chem. Soc.* **2010**, *132*, 12983−12990.

DOI: 10.1021/acs.inorgchem.9b01592
Inorg. Chem. 2019, 58, 13815−13825